Computation of Resting State Networks from fMRI Through A Measure of Phase Synchrony

Marisel Villafañe-Delgado[1], David C. Zhu[2] and Selin Aviyente[1]

***Abstract*— Resting-state fMRI (rs-fMRI) studies of the human brain have demonstrated that low-frequency fluctuations can define functionally relevant resting state networks (RSNs). The majority of these methods rely on Pearson's correlation for quantifying the functional connectivity between the time series from different regions. However, it is well-known that correlation is limited to quantifying only linear relationships between the time series and assumes stationarity of the underlying processes. Many empirical studies indicate nonstationarity of the BOLD signals. In this paper, we adapt a measure of time-varying phase synchrony to quantify the functional connectivity and modify it to distinguish between synchronization and desynchronization. The proposed measure is compared to the conventional Pearson's correlation method for rs-fMRI analyses on two subjects (six scans per subject) in terms of their reproducibility.**

I. INTRODUCTION

Resting-state functional magnetic resonance imaging (rs-fMRI) studies of functional connectivity has contributed greatly to the definition of functional networks and the assessment of neurological disorders [1], [2]. Various resting-state networks have been consistently defined among subjects, such as the default mode-network (DMN), the sensory-motor network, and visual network. Resting-state networks (RSNs) generated from rs-fMRI present promising potentials in clinical applications. For example, the research in RSNs may potentially lead to the early detection of Alzheimer's disease [3].

Current techniques employed in the definition of fMRI RSNs include independent component analysis, wavelet coherence, and seed-based correlations [4]. Although it remains as a popular method, linear correlation does not take into account the nonlinear structure of blood-oxygen level-dependent (BOLD) responses measured by fMRI. Also, as in the case of rs-fMRI, BOLD responses need to be band-pass filtered in a narrowband of frequencies typically between 0.01 Hz and 0.1 Hz before computation of correlation coefficient and are assumed to be stationary.

Phase synchrony presents an alternative to Pearson's correlation-based analysis in rs-fMRI. It has been applied to fMRI data as a method for detecting activation [5] and more recently for connectivity analysis in rs-fMRI [6]. These studies have estimated the instantaneous phase from the Hilbert transform of narrowband filtered signals. This approach requires prefiltering of the signals and does not provide a high time-frequency resolution for phase synchrony estimates. In this paper, we propose the identification of RSNs using Reduced-Interference Rihaczek (RID-Rihaczek) time frequency distribution based phase synchrony measures [7]. Recent work showed that this technique yielded better resolution and increased robustness to noise compared to other phase synchrony estimation methods [8]. In addition, this method does not require bandpass filtering of the data prior to the estimation of the instantaneous phase and provides a full time-frequency map of synchronization.

The rest of this paper is organized as follows. Section II will describe the Rihaczek-based phase synchrony measure and its modification to differentiate synchronization from desynchronization, fMRI data acquisition and preprocessing, and statistical significance testing. Section III will include the results of the comparison between the original phase synchrony analysis and its modified version, and the connectivity of the DMN and visual network based on the proposed method. Moreover, the reproducibility of the proposed method will be compared to Pearson's correlation method across six scans for two subjects.

II. METHODS

A. Time-Frequency Phase Synchrony (TFPS)

In this paper, we quantify the functional connectivity using a recent phase synchrony measure based on the RID-Rihaczek distribution [8]. First, we quantify the time varying phase of a signal, $\Phi_i(t,\omega)$ as $\Phi_i(t,\omega) = \arg\left[\frac{C_i(t,\omega)}{|C_i(t,\omega)|}\right]$ where $C_i(t,\omega)$ is the complex RID-Rihaczek distribution belonging to Cohen's class of quadratic time-frequency distributions [1]:

$$C_i(t,\omega) = \int\int \underbrace{\exp\left(-\frac{(\theta\tau)^2}{\sigma}\right)}_{\text{Choi-Williams kernel}} \underbrace{\exp(j\frac{\theta\tau}{2})}_{\text{Rihaczek kernel}} A_i(\theta,\tau) e^{-j(\theta t+\tau\omega)} d\tau d\theta, \quad (1)$$

and $A_i(\theta,\tau) = \int s_i(u+\frac{\tau}{2}) s_i^*(u-\frac{\tau}{2}) e^{j\theta u} du$ is the ambiguity function of the time series s_i. The phase synchrony between two regions of interest i and j at time t and frequency ω is computed using Phase Locking Value (PLV):

$$PLV_{i,j}(t,\omega) = \frac{1}{2\Delta+1}\left|\int_{t-\Delta}^{t+\Delta} \exp\left(j\Phi_{i,j}(\tau,\omega)\right) d\tau\right| \quad (2)$$

*This work was in part supported by the National Science Foundation under Grant No. DGE-1424871 and the MSU Radiology Pilot Scan Program

[1]M. Villafañe-Delgado and S. Aviyente are with the Department of Electrical and Computer Engineering, Michigan State University, East Lansing, MI, 48824 aviyente@egr.msu.edu

[2]D. C. Zhu is with the Department of Radiology, Michigan State University, East Lansing, MI, 48824

[1]The details of the RID-Rihaczek distribution and the corresponding synchrony measure are given in [8].

978-1-4244-7929-0/14/$26.00 ©2014 IEEE

where $2\Delta+1$ is the length of the time-window over which the consistency of the phase difference $\Phi_{i,j}(t,\omega) = |\Phi_i(t,\omega) - \Phi_j(t,\omega)|$ is computed. The value of Δ depends on the characteristics of the signal and its sampling rate. A small value of Δ will provide good time localization at the expense of increasing the variance of the phase synchrony estimates while a large value of Δ cannot capture the nonstationary variations. In this paper, we investigate the effect of Δ on the estimated functional connectivity and the reproducibility of the resulting RSNs.

B. Modified PLV

One shortcoming of standard synchrony measures is the lack of discrimination between synchronization and desynchronization. For example, if two signals have a constant phase difference of 0^0 or 180^0, in both cases the computed PLV will be equal to 1 in the original method. In order to differentiate between the different phase angles, we propose a modification to the original method in which the PLV at each time and frequency is weighted by the cosine of the angle of the average phase difference in the $2\Delta + 1$ time-window, as described by Equation 3.

$$\widetilde{PLV}_{i,j}(t,\omega) = PLV_{i,j}(t,\omega) \cos\left(arg\left[\int_{t-\Delta}^{t+\Delta} \exp\left(j\Phi_{i,j}(\tau,\omega)\right)d\tau\right]\right) \quad (3)$$

C. fMRI data

Two college students (one 28-year old male and one 30-year old female) participated in this study. Both subjects self-reported that they were free of neurological disorders. Both subjects signed consent forms approved by the Michigan State University Institutional Review Board.

The experiment was conducted on a GE 3T Signa® HDx MR scanner (GE Healthcare, Waukesha, WI) with an 8-channel head coil. A 7-min rs-fMRI run was repeated six times. For each 7-min rs-fMRI run, echo-planar images, starting from the most inferior regions of the brain, were acquired with the following parameters: 36 contiguous 3-mm axial slices in an interleaved order, time of echo (TE) = 27.7 ms, time of repetition (TR) = 2500 ms, flip angle = 80°, field of view (FOV) = 22 cm, matrix size = 64x64, ramp sampling, and with the first four data points discarded. Each volume of slices was acquired 164 times while a subject was asked to relax and keep his/her eyes closed. Then high-resolution isotropic ($1mm^3$) T_1-weighted volumetric inversion recovery fast spoiled gradient-recalled images with cerebrospinal fluid suppressed were obtained to cover the whole brain.

Resting-state fMRI pre-processing was conducted using AFNI software in the native space. For each subject, the acquisition timing difference was first corrected for different slice locations. With the last functional volume as the reference, rigid-body motion correction was done in three translational and three rotational directions. For each subject, spatial blurring with a full width half maximum (FWHM) of 4 mm was used to reduce random noise. At each voxel, motion-estimation parameters, baseline, linear and quadratic system-induced signal trends were removed from the time courses. Brain global, CSF and white matter (WM) mean signals were modeled as nuisance variables and removed from the time courses as well. The cleaned time courses were then band-pass filtered between 0.009 Hz and 0.08 Hz [2]. These filtered time courses were used for correlation-based connectivity analyses.

The cortical nodes of the DMN were extracted from the functional networks produced by [9] based on rs-fMRI datasets from 1,000 healthy young adults. The group averaged cortical surface map of DMN was provided in FreeSurfer [10]. We segmented this surface map to the following eight nodes according to the clustering characteristics and anatomical region: right and left posterior cingulate cortices (PCC), right and left anterior cingulate cortices (ACC)/medial frontal cortices (MeFC), right and left superior frontal gyri (SFG), and right and left inferior parietal lobules (IPL)/angular gyri (AG). The Medial Temporal Lobe (MTL), where hippocampus is the core, is often considered part of the DMN [11]. The space-averaged filtered time course described earlier was generated at each node, including hippocampus. For comparison, two nodes of the visual network (right and left lateral occipital cortices) were extracted based on FreeSurfer [10].

D. Statistical Significance Testing

Tests for statistically significant synchronization are based on nonparametric permutation tests and accounting for multiple comparisons from the false discovery rate. A total of 500 surrogate time series are generated using circular shift bootstrapping [12]. For a time series x_i, $i = 1, ..., N$, N blocks, $B_1, ..., B_N$ are constructed with each block containing b elements and defined as $B_i = x_i, ..., x_{i+b-1}$. Next, k blocks are selected randomly from the set B_1, ...,B_N, where k satisfies $kb \approx N$. The length b of each block is chosen such that the mean square error of the estimator of the long-run variance is minimized [13]. The selected k blocks are concatenated to construct a surrogate time series.

Tests for multiple comparisons tests are based on the false discovery rate [14]. First, p-values are estimated for the average synchrony in the 0.009-0.08 Hz frequency band by the empirical distribution from the surrogate data set. Next, for a total of V pair-wise comparisons their corresponding p-values are sorted in increasing order $P_{(1)} \leq P_{(2)} \leq ... \leq P_{(V)}$. The goal is to define r to be equal to i for which $P_{(i)} \leq \frac{i}{V}\frac{q}{C(V)}$ where $q \in [0,1]$ sets the maximum false discovery rate desired and $C(V) = \sum_{i=1}^{V} \frac{1}{i}$. Finally, pair-wise comparisons $V_{(1)}, ..., V_{(r)}$ are declared to be statistically significantly synchronized. In this work a q of 0.1 is selected as suggested by [14] for fMRI data.

III. Results

In this section, first the modified PLV is compared to the original PLV. Figure 1 (a) and (b) show the time-frequency synchronization between the left hippocampus and right

ACC/MeFC for the original and modified PLV, respectively, for Subject 1, run 1. Here $\Delta = 7$ or, equivalently, a window of 37.5 seconds. As expected, the modified PLV measure detects synchronization and desynchronization for instances when the original PLV shows only high synchrony. It can also be noted from these time-frequency maps that there is a stronger synchrony for frequencies below 0.1 Hz, the frequency range of the rs-fMRI signal assumed to contribute to RSNs.

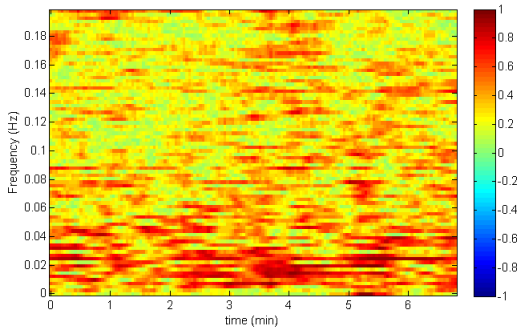

(a) Original PLV measure.

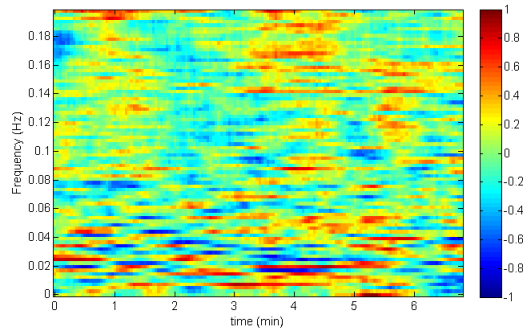

(b) Modified PLV measure.

Fig. 1: Phase synchrony between left hippocampus and right ACC/MeFC calculated based on the (a) original and (b) modified PLV method.

Next, the strength of connectivity among regions within the DMN was estimated using Pearson's correlation and the modified PLV. Synchrony based on the modified PLV was obtained by averaging $\widetilde{PLV}_{i,j}(t,\omega)$ over the frequency bins corresponding to frequencies 0.009 Hz-0.08 Hz across all time. Figure 2 (a) and (b) show the connectivity matrix estimated from the modified PLV and Pearson's correlation, respectively, for run 5 from subject 2. After correction for multiple comparisons the corrected p-value was found to be 0.01. The modified PLV produces comparable results in the estimation of the connectivity of DMN nodes. For example, both methods exhibit strong connectivity between the right and left PCC, right and left ACC/MeFC. From Figure 2 (a) lateral occipital regions are not found to be statistically significantly synchronized to nodes of the DMN except for the right IPL/AG and hipppocampus. This is comparable to anti-correlations and no significant connectivity found from the Pearson's correlation method.

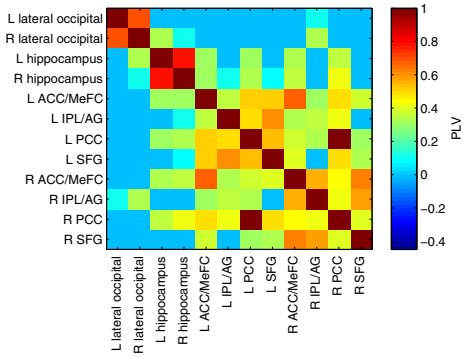

(a) Modified PLV

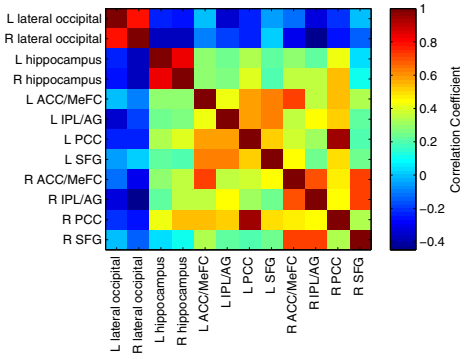

(b) Pearson's Correlation

Fig. 2: Significant connectivity matrix for Subject 2, Run 5: (a) Modified PLV, (b) Pearson's Correlation.

We also investigated the effect of windows sizes in the correlation and synchrony estimates. For this purpose, first we selected two regions that exhibit significant synchrony, the right and left IPL/AG, and computed the sliding window correlation with one sample increments (2.5 s) and PLV between them. Figure 3 shows the time courses of correlation and phase synchrony averaged over all runs and two subjects. Window sizes consist of 4, 8, and 16 samples (10 s, 20 s, and 40 s) and Δ values of 2, 4, and 7 equivalent to windows of 12.5 s, 22.5 s, and 37.5 s. In general, although both techniques follow similar patterns of synchronization over time, synchrony based on Pearson's correlation exhibits higher frequency fluctuations in connectivity across time compared to PLV, which is smoother for all window sizes due to the filtering provided by RID-Rihaczek. Finally, the time courses of Pearson Correlation and PLV are highly correlated, especially for larger window sizes.

Finally, we investigated the variation in synchronization across scans between right and left IPL/AG, and left PCC and left ACC/MeFC. Table 1 shows the mean$\pm$standard deviation and % of variation for the same Δ and window lengths as for Figure 3. For both subjects and all windows considered the PLV shows higher variation than correlation, however it

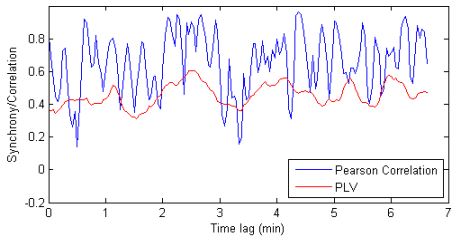

(a) Window length = 4 / Δ = 2

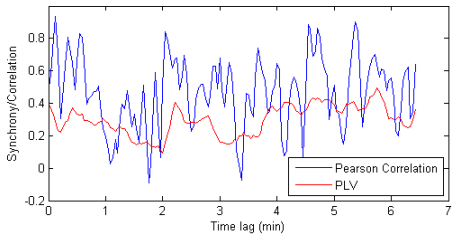

(b) Window length = 8 / Δ = 4

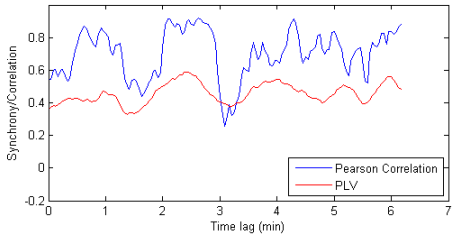

(c) Window length = 16 / Δ = 7

Fig. 3: Effect of windows sizes in the correlation and synchrony estimates.

does not fluctuate much due to changes in window length. A similar trend can also be found with other pairs of the DMN, and the pair of left and right lateral occipital cortices.

IV. CONCLUSIONS

A modified version of phase synchrony is presented based on the complex RID-Rihaczek time-frequency distribution as an alternative approach to Pearson's correlation in the computation of RSN connectivity from rs-fMRI. This method can estimate both synchronization and desynchronization as a function of time and frequency between fMRI time series. It generated comparable results to Pearson's correlation within the nodes of the DMN. It is also more immune to the choice of sliding window length than the Pearson's correlation method in connectivity estimation. Its measurement offers a direct way of quantifying time-varying connectivity and can potentially be used to investigate dynamic functional connectivity in fMRI time series and the characterization of connectivity patterns.

TABLE I: Variability of Modified PLV and Pearson's Correlation Affected by Sliding Window Length across Six Runs of fMRI Dataset

Connection Pair	Delta/ Window	PLV Subject 1/Subject 2	Correlation Coefficient Subject 1/Subject 2
R IPL/AG – L IPL/AG	2/4	0.445±0.125(28.1%)/ 0.293±0.131(44.8%)	0.657±0.130(19.8%)/ 0.480±0.225(46.9%)
	4/8	0.435±0.122(28.1%)/ 0.283±0.129(45.6%)	0.713±0.128(18.0%)/ 0.540±0.191(35.4%)
	7/16	0.420±0.118(28.1%)/ 0.272±0.126(46.3%)	0.727±0.114(15.7%)/ 0.593±0.178(30.0%)
L PCC – L ACC/MeFC	2/4	0.265±0.100(37.9%)/ 0.224±0.177(79.1%)	0.481±0.110(23.3%)/ 0.363±0.224(61.6%)
	4/8	0.258±0.100(38.7%)/ 0.218±0.174(79.7%)	0.545±0.093(17.0%)/ 0.373±0.216(58.1%)
	7/16	0.248±0.098(39.6%)/ 0.210±0.168(80.0%)	0.567±0.109(19.3%)/ 0.380±0.223(58.7%)

Numbers shown are in mean±standard deviation (variation%). variation% = the ratio of standard deviation over absolute mean in percentage. R = right, L = left.

REFERENCES

[1] M. N. Moussa, M. R. Steen, P. J. Laurienti, and S. Hayasaka, "Consistency of network modules in resting-state fmri connectome data," *PloS one*, vol. 7, no. 8, p. e44428, 2012.

[2] M. D. Fox, A. Z. Snyder, J. L. Vincent, M. Corbetta, D. C. Van Essen, and M. E. Raichle, "The human brain is intrinsically organized into dynamic, anticorrelated functional networks," *Proceedings of the National Academy of Sciences of the United States of America*, vol. 102, no. 27, pp. 9673–9678, 2005.

[3] D. C. Zhu, S. Majumdar, I. O. Korolev, K. L. Berger, and A. C. Bozoki, "Alzheimer's disease and amnestic mild cognitive impairment weaken connections within the default-mode network: a multi-modal imaging study," *Journal of Alzheimer's Disease*, vol. 34, no. 4, pp. 969–984, 2013.

[4] D. M. Cole, S. M. Smith, and C. F. Beckmann, "Advances and pitfalls in the analysis and interpretation of resting-state fmri data," *Frontiers in systems neuroscience*, vol. 4, p. 8, 2010.

[5] A. R. Laird, B. P. Rogers, J. D. Carew, K. Arfanakis, C. H. Moritz, and M. E. Meyerand, "Characterizing instantaneous phase relationships in whole-brain fmri activation data," *Human brain mapping*, vol. 16, no. 2, pp. 71–80, 2002.

[6] E. Glerean, J. Salmi, J. M. Lahnakoski, I. P. Jääskeläinen, and M. Sams, "Functional magnetic resonance imaging phase synchronization as a measure of dynamic functional connectivity," *Brain connectivity*, vol. 2, no. 2, pp. 91–101, 2012.

[7] S. Aviyente, E. M. Bernat, W. S. Evans, and S. R. Sponheim, "A phase synchrony measure for quantifying dynamic functional integration in the brain," *Human brain mapping*, vol. 32, no. 1, pp. 80–93, 2011.

[8] S. Aviyente and A. Y. Mutlu, "A time-frequency-based approach to phase and phase synchrony estimation," *Signal Processing, IEEE Transactions on*, vol. 59, no. 7, pp. 3086–3098, 2011.

[9] B. T. Yeo, F. M. Krienen, J. Sepulcre, M. R. Sabuncu, D. Lashkari, M. Hollinshead, J. L. Roffman, J. W. Smoller, L. Zöllei, J. R. Polimeni *et al.*, "The organization of the human cerebral cortex estimated by intrinsic functional connectivity," *Journal of neurophysiology*, vol. 106, no. 3, pp. 1125–1165, 2011.

[10] B. Fischl, D. H. Salat, E. Busa, M. Albert, M. Dieterich, C. Haselgrove, A. van der Kouwe, R. Killiany, D. Kennedy, S. Klaveness *et al.*, "Whole brain segmentation: automated labeling of neuroanatomical structures in the human brain," *Neuron*, vol. 33, no. 3, pp. 341–355, 2002.

[11] R. L. Buckner, J. R. Andrews-Hanna, and D. L. Schacter, "The brain's default network," *Annals of the New York Academy of Sciences*, vol. 1124, no. 1, pp. 1–38, 2008.

[12] D. N. Politis and J. P. Romano, "A circular block-resampling procedure for stationary data," *Exploring the limits of bootstrap*, pp. 263–270, 1992.

[13] D. N. Politis and H. White, "Automatic block-length selection for the dependent bootstrap," *Econometric Reviews*, vol. 23, no. 1, pp. 53–70, 2004.

[14] C. R. Genovese, N. A. Lazar, and T. Nichols, "Thresholding of statistical maps in functional neuroimaging using the false discovery rate," *Neuroimage*, vol. 15, no. 4, pp. 870–878, 2002.